This is a repository copy of *Photonic integration of uniform GaAs nanowires in hexagonal and honeycomb lattice for broadband optical absorption*.

White Rose Research Online URL for this paper:
http://eprints.whiterose.ac.uk/167040/

Version: Published Version

White Rose
university consortium
Universities of Leeds, Sheffield & York

eprints@whiterose.ac.uk
https://eprints.whiterose.ac.uk/

Photonic integration of uniform GaAs nanowires in hexagonal and honeycomb lattice for broadband optical absorption

Saraswati Behera (iD), Paul W. Fry, Henry Francis (iD), I. Farrer (iD), Chaoyuan Jin (iD), and Mark Hopkinson (iD)

View Online   Export Citation   CrossMark

ARTICLES YOU MAY BE INTERESTED IN

Photonic integration of uniform GaAs nanowires in hexagonal and honeycomb lattice for broadband optical absorption

Saraswati Behera,[a] [iD] Paul W. Fry, Henry Francis, [iD] I. Farrer, [iD] Chaoyuan Jin, [iD] and Mark Hopkinson [iD]

AFFILIATIONS

Department of Electronics and Electrical Engineering, University of Sheffield, Sheffield S3 7HQ, United Kingdom

[a]Author to whom correspondence should be addressed: s.behera@sheffield.ac.uk

ABSTRACT

We present an experimental approach toward the realization of GaAs nanowires in the form of square, hexagonal, and honeycomb lattices for photonic integration toward enhanced optical properties. We have carried out a design and fabrication process on GaAs wafers using electron beam lithography patterning, reactive ion etching for hard mask removal, and inductively coupled plasma etching of the material. The resulting photonic crystals are analyzed by field emission scanning electron microscopy. Nanowire array designs in a square, hexagonal, and honeycomb lattice with a variable height of nanowires have been studied. Using finite-difference time-domain simulation, we can derive the comparative optical absorption properties of these nanowire arrays. A very high broadband absorbance of >94% over the 400 nm–1000 nm wavelength range is studied for hexagonal and honeycomb arrays, while a square lattice array shows only a maximum of 85% absorption. We report a minimum of 2% reflectance, or 98% optical absorbance, over 450 nm–700 nm and over a wide angle of 45° through hexagonal and honeycomb lattice integration in GaAs. These results will have potential applications toward broadband optical absorption or light trapping in solar energy harvesting.

I. INTRODUCTION

Ordered and disordered nanowires are an active area of photonics research covering a wide range of semiconductor applications, such as solar cells, light-emitting diodes, lasers, and optical circuit components.[1–7] Photonics-based bandgap tunability is an important aspect of the integration of photonic designs to semiconductor materials to enable unique optoelectronic properties.[8] Photonics integration has also played an advantageous role in broadening the bandgap dependent narrowband operation of semiconductors to utilize a broader solar spectrum.[9] In nanowires, a large surface to volume ratio and reduction in refractive index contrast between the semiconductor and air allows photonics-based waveguiding and the confinement of modes within photonic crystals.

For ordered 2D nanowires, there is mode confinement along the XY plane and a free space propagation of selective confined modes along the third direction.[10] In the case of disordered/random nanowires, wavelength broadening takes place due to the overlap of an asymmetric bandgap.[10] Similarly, a photonic quasicrystal shows a completely symmetric and omnidirectional bandgap in 2D photonics.[11] This type of quasiperiodic photonics integration has been implemented in silicon photonics toward solar photovoltaics by Xavier *et al.*[12] Considering GaAs single-junction thin-film solar cells, these have achieved a maximum solar conversion efficiency of up to 28% so far.[13] A photonic integration to GaAs would be advantageous for efficiency enhancement through broad optical absorption.

Nanowires based on semiconductors, specifically, GaAs, have been widely studied for various optoelectronic applications such as in light-emitting diodes,[14,15] solar cells,[16–18] and photodetectors.[19] In general, semiconductor nanowire structures with typically <200 nm diameter and one to a few micrometers of axial length can allow electromagnetic wave localization along the XY plane. These structures can be grown using various growth techniques such as vapor–liquid–solid (VLS) growth by molecular

beam epitaxy (MBE)[20–22] or by selective area metalorganic vapor phase epitaxy (MOVPE).[23,24] Although these techniques are well-established in semiconductor technology, the uniformity and one-to-one lattice-site periodic growth of nanowires are very much dependent upon the lattice orientation with respect to the substrate crystal.

Moreover, the possibility of several photonic kinds of crystal orientation on the same substrate is a challenge through these techniques. A periodic patterning possibility would add versatility to the semiconductor-photonic integration exploring wide applications. Nanoimprint lithography followed by MBE growth has been used to obtain periodic growth of nanowires.[25] However, this technique needs a mold for which the design parameters are fixed, and there is no indication that this technique can produce nanowires of sub-micron scale lattice pitch, which is needed for visible spectrum applications. Period patterning down to sub-micron scales is possible using laser interference lithography (IL). This is a relatively simple, large area, low-cost and rapid fabrication approach;[26–29] however, it needs a lot of process optimization based on the threshold of laser power as well as photoresist thickness. To achieve more complex photonic structure patterning requires a phase spatial light modulator-based phase-engineered IL technique.[30–34]

Therefore, in the current study, for showing the initial possibilities of photonic integration to III–V semiconductor technology, we have followed the electron beam lithography (EBL)-based design and fabrication technique that allows us complete flexibility over a single exposure.[35,36] This periodic patterning scheme can further be implemented in any semiconductor material to obtain periodic nanowires based on specific lattice design parameters for suitable applications.

This study is aimed at the design and fabrication of interfaces for enhanced photonic wave guidance and light trapping toward absorption enhancement. The uniform density and design scalability can be achieved through patterning a SiO$_2$ coated GaAs substrate using electron-beam lithography followed by plasma etching tools. In this work, we present different uniform photonic nanostructuring schemes in GaAs for enabling broadband absorption from the UV–NIR wavelength range. We present square lattice, hexagonal lattice, and honeycomb lattice-based photonic GaAs nanowire designs, simulations, and fabrication approaches. Finite-difference time-domain (FDTD) based simulation studies are carried out to show the optical absorption properties of GaAs nanowires in photonic lattices and the advantages of different lattice arrangements over the basic square lattice for enhanced light trapping possibilities. Electron beam lithography and material processing through plasma tools are presented to outline the possibilities for experimental realization.

II. FDTD SIMULATION

We have carried out FDTD-based simulation studies using Lumerical solutions FDTD module on the optical properties of the patterned GaAs nanowire arrays and compared the results of a basic square lattice to those of the hexagonal and honeycomb lattices to examine the preferred design of the GaAs nanowire arrays for fabrication. We have simulated three different lattice design models in FDTD, as shown in Figs. 1(a)–1(c). The diameter of the nanowires (d) is 180 nm, the periodicity of a square lattice is 400 nm, and the axial height (Z span) is varied as 500 nm–2500 nm for maximization of optical absorbance. We use a plane
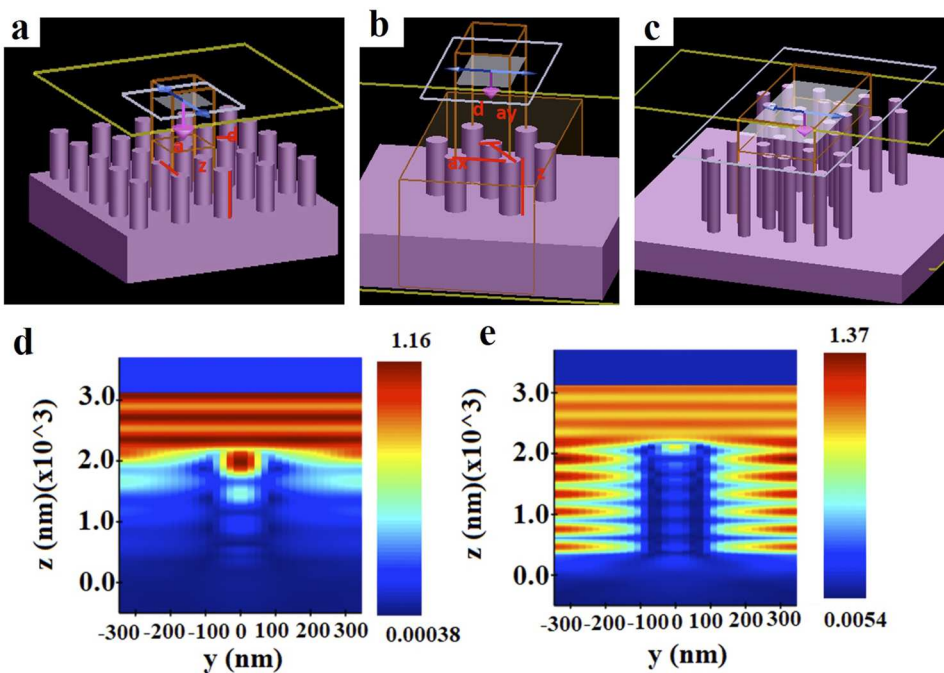
FIG. 1. FDTD simulation model: (a) square lattice with periodicity a = 400 nm, (b) hexagonal lattice with periodicities a$_x$ = 400 nm and a$_y$ = 346.41, (c) honeycomb lattice with a$_x$ = 800 and a$_y$ = 692.81 nm. [(d) and (e)] Electric field distribution in the YZ plane at two different wavelengths 727 nm and 567 nm showing light trapping due to photonic crystal based wave-guiding.

wave source with the broadband wavelength covering 400 nm–1000 nm incident along the Z direction. Absorbance is calculated as A = 1 − (R + T). The electric field distributions through the GaAs nanowire photonic crystal showing electromagnetic energy trapping through photonic crystal-based waveguiding are presented in Figs. 1(d) and 1(e) at two different wavelengths 727 nm and 567 nm. This image indicates that the electric field is localized inside the air medium for higher wavelengths and is localized inside the nanowires for lower wavelengths contributing to broad-spectrum electromagnetic field absorption inside the GaAs/air photonic crystal.

In the case of a square lattice, we observe 69% of optical absorbance over 400 nm–1000 nm for 500 nm height of the nanowires and an 80% absorbance for a Z span of 1 μm of the nanowires, which then increases to 85% in the case of a Z span of 2 μm followed by 75% for 2.5 μm as shown in Fig. 2(a).

The absorbance is enhanced to 90%, 93%, and 95% for 500 nm, 1 μm, and 2 μm of Z spans, respectively, in the case of hexagonal lattice over a broad spectrum of 400 nm–1000 nm, as shown in Fig. 2(b). This improvement is due to in-plane lattice symmetry in the hexagonal lattice in comparison to the square lattice. Furthermore,, we have extended such a study to include a honeycomb lattice. The honeycomb lattice design shows the maximum absorbance among all the periodic lattice arrangements we have studied, with values of 90%, 94%, and 95% optical absorptions over 400 nm–1000 nm wavelength range for 500 nm, 1 μm, and 2 μm height of the nanowires, respectively, as shown in Fig. 2(c). The GaAs nanowires in a honeycomb lattice with 2 μm height show a maximum optical absorbance of 95% and a total optical absorption power of 85% inside the

substrate through the nanophotonic scheme over the broad solar spectrum.

We conclude that the hexagonal and honeycomb lattice designs are much preferred over the square lattice-based designs for broadband absorption enhancement in GaAs uniform nanowire arrays for solar cell applications. It is also inferred that although the nanowires with a maximum Z span of 2 μm show improved absorbance, the change in absorbance with respect to the Z span is not significant. Therefore, for a low-cost fabrication approach that includes lesser material, processing time, and fabrication feasibility, we propose the design of hexagonal and honeycomb lattices with a Z span of 1 μm–2 μm as the preferred design for solar cell applications.

III. EXPERIMENT

We have fabricated square, hexagonal, and honeycomb lattice-based GaAs nanowire arrays using the fabrication steps as presented in Fig. 3. We have deposited a silicon dioxide (SiO$_2$) hard mask of 300 nm–400 nm over the GaAs substrate using PECVD for 5 min. The substrate is spun with an electron beam resist, which is then exposed with designed patterns. The exposed sample is developed and cleaned. The patterned substrate is etched with reactive ion etching (RIE) for 19 min with CHF$_3$ flow to obtain the pattering in SiO$_2$.

The residual resist is removed by placing the sample in the resist remover solution for 5 min, and the sample is then oxygen plasma treated for 5 min to remove residual organics and to obtain a clean photonic crystal in SiO$_2$/air. Subsequently, the sample is inductively coupled plasma (ICP) etched in the presence of chlorine and argon gas for 3 min–5 min to etch the GaAs through the hard mask. The
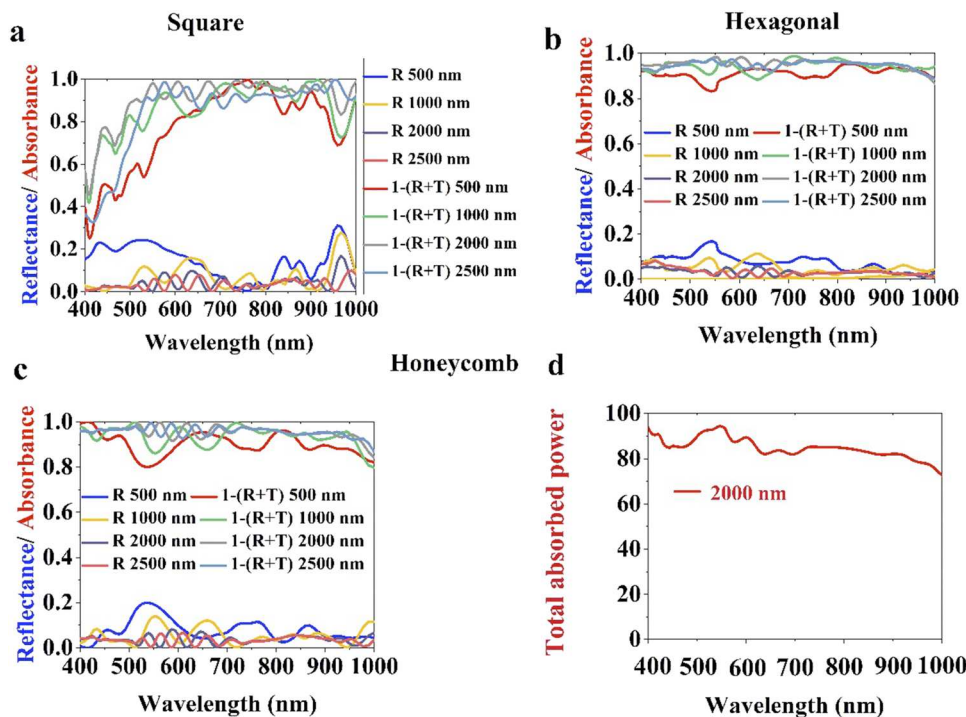
FIG. 2. FDTD simulation studied optical absorbance properties of the GaAs nanowire array of variable height in the case of (a) square lattice, (b) hexagonal lattice, and (c) honeycomb lattice. (d) Calculated total optical power absorbed (86%) due to the honeycomb lattice of 2000 nm height showing an absorbance of 95% over the 400 nm–1000 nm broad wavelength range.
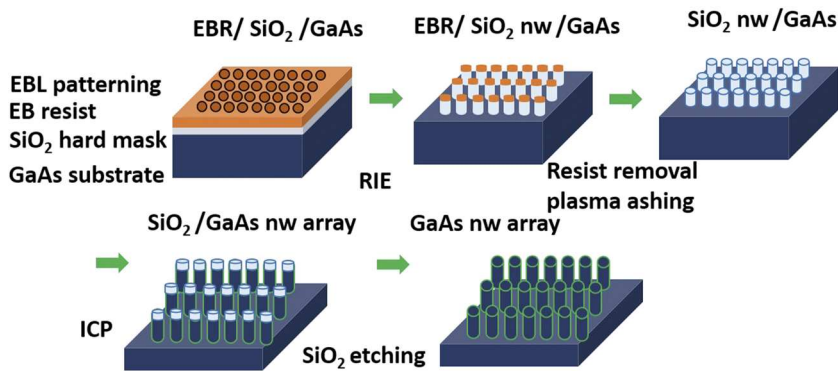
FIG. 3. Steps for experimental realization of the photonic integrated GaAs nanowire array through electron beam lithography-based patterning, RIE, ICP, and HF etching.

etched GaAs sample is further etched with HF to remove the SiO$_2$ hard mask. The realized photonic structure in the GaAs is presented in Figs. 4–6. A brief description of the experimental techniques is presented in Sec. V.

A. Square lattice

We carried out electron beam lithography-based nanoscale patterning and reactive ion etching on the samples as per the above steps presented in Fig. 3 to obtain photonic crystals of a square, hexagonal, and honeycomb lattice on GaAs/air. The surface analysis studies through scanning electron microscopy are presented in Figs. 4–6. Figure 4 presents the square lattice patterns obtained

through electron beam lithography. As evidenced in Fig. 4(a), for a designed diameter of 320 nm in the square lattice pattern, we could verify from the surface morphology the existence of large area and uniform square lattice photonic structures. The magnified images in Figs. 4(b) and 4(c) show uniform square lattice patterns of ~278 nm diameter present over 405 nm lattice spacing. We have carried out ICP etching of the SiO$_2$ underlying GaAs samples for 3 min, and the surface morphology of the etched samples is presented in Figs. 4(d)–4(f). Figure 4(d) shows a cross-sectional SEM image view presenting GaAs nanowires of 300 nm–400 nm height for a design diameter of 320 nm diameter. Furthermore, GaAs nanopillars of 240 nm diameter are shown in Fig. 4(e). A higher dose electron beam exposure for 240 nm shows the anisotropic etching of the GaAs nanowires that
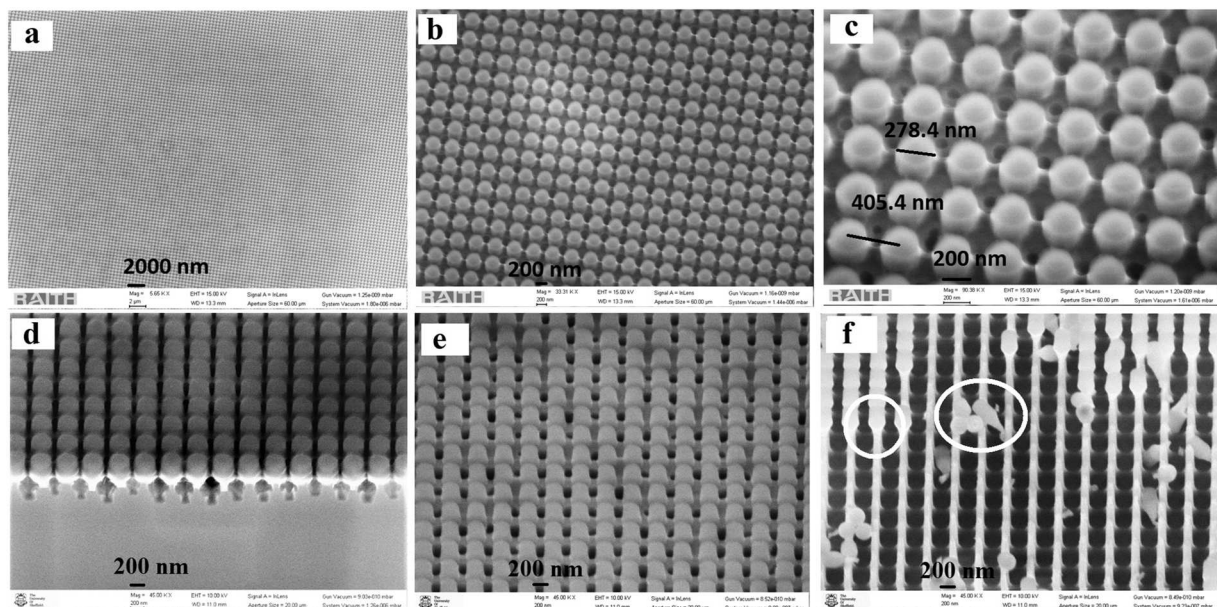
FIG. 4. SEM images of the experimentally observed square lattice (periodicity = 400 nm) on SiO$_2$ with the designed parameters of diameter 320 nm showing uniform distribution {(a) large area view and [(b) and (c)] magnified view}. GaAs nanowires after ICP etching of 3 min: (d) cross-sectional views of the SEM images for the diameter of 320 nm showing pillars of height approximately 300 nm–400 nm and [(e) and (f)] for the diameter of 240 nm for higher exposure doses of the electron beam where the encircled region shows non-uniform etching in higher doses leading to tapered nanowires.
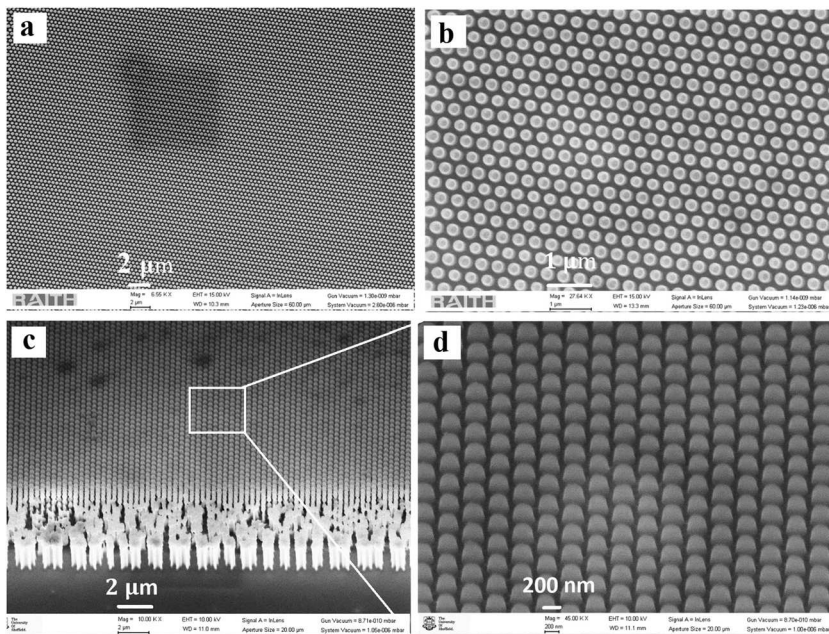
FIG. 5. SEM images of the experimentally observed hexagonal lattice [periodicity (ax) = 400 nm, ay = 343.41 nm] with the designed parameters of diameter 240 nm showing uniform distribution [(a) large area image and (b) magnified image]. (c) Cross-sectional views of the SEM images for a diameter of 240 nm and (d) magnified image in a cross-sectional view.
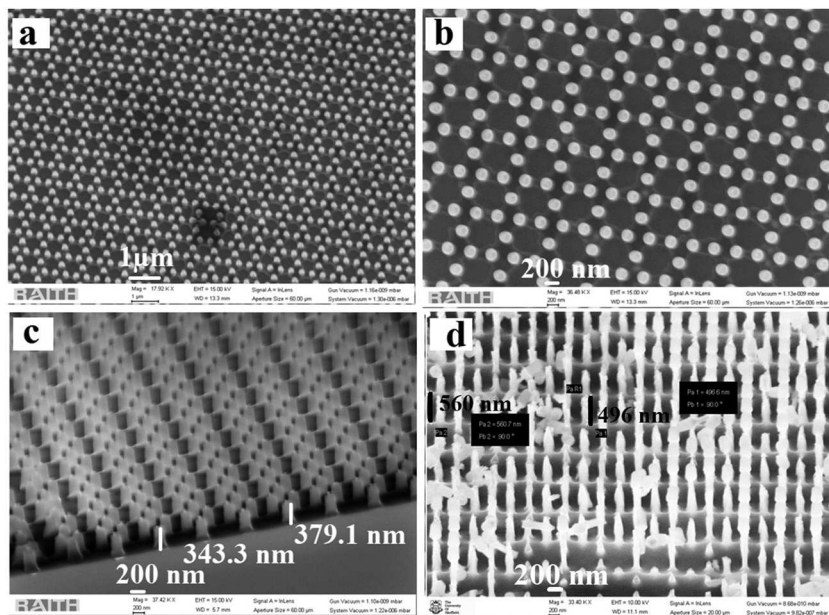
FIG. 6. SEM images of the experimentally observed honeycomb lattice on SiO_2 [periodicity (ax) = 800 nm, ay = 692.82 nm] with the designed parameters of diameter 180 nm showing uniform distribution [(a) large area image and (b) magnified view]. (c) Cross-sectional views of the SEM images for a diameter of 180 nm and (d) top-surface view of the 3 min ICP etched samples showing GaAs nanopillars of height ~500 to 556.

are tapered in some regions as encircled of comparatively thinner diameter nanowires in the rest of the regions, as shown in Fig. 4(f). This is a result of anisotropic etching in several doses of the electron beam exposure depending upon the diameter of the designs and etching rate.[37]

B. Hexagonal lattice

In the case of hexagonal nanowires, we used design diameters of 180 nm and 240 nm. The results show good uniformity for a periodicity of 240 nm as observed from Fig. 5(a) over a relatively large area. The magnified and 20° tilted views of the SEM images show hexagonally arranged periodic lattices of approximate height 116 nm, as presented in Fig. 5(b). Furthermore, we have ICP etched the samples for 3 min. The SEM images of the ICP etched samples are shown in Figs. 5(c) and 5(d).

C. Honeycomb lattice

In the case of the realized honeycomb lattice, we could observe uniformly distributed nanopillars for d = 180 nm in SiO_2, as shown
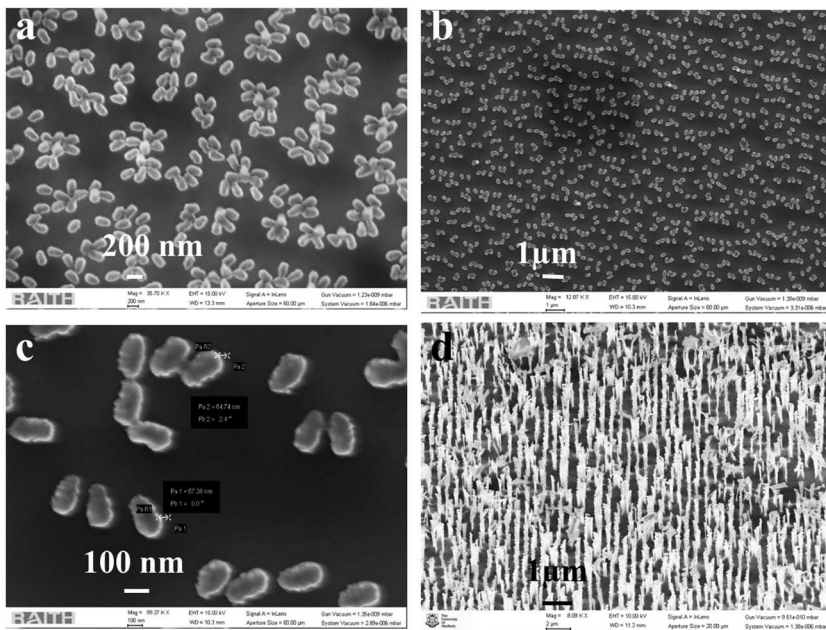
FIG. 7. SEM images of random GaAs patterns obtained after ICP etching in the case of (a) square lattice with diameter 180 nm, (b) hexagonal lattice with diameter 180 nm, (c) magnified view of the random pattern from the hexagonal lattice, and (d) honeycomb lattice with diameter 240 nm showing denser and near uniform anisotropic nanowires compared to square and hexagonal lattices.

in Figs. 6(a) and 6(b) through the low and high magnification SEM images. As observed from the cross-sectional view of the SEM image in Fig. 6(c), we see honeycomb patterns of height approximately 350 nm in the SiO₂ hard mask. Upon ICP etching of the underlying GaAs, followed by hard mask removal through HF, we could obtain GaAs nanopillars of ~500 nm to 560 nm height, as shown in Fig. 6(d).

D. Aperiodic lattice/random pattern

We experimentally observe random patterns for a square lattice designed with 180 nm diameter through EBL as shown in Fig. 7(a) due to a higher etching rate through the space between the lattice period and the patterned region. Similarly, we also obtain random patterns in the case of hexagonal lattice after ICP etching, as shown in Figs. 7(b) and 7(c). However, it is reverse phenomena in the case of honeycomb lattice. In the case of honeycomb lattice, we obtain uniformity in the case of diameter 180 nm and we obtain random patterns for a higher diameter of 240 nm, as shown in Fig. 7(d). However, in the case of aperiodic honeycomb lattice, the density of

the patterning region is high and we obtain anisotropic nanowires of more than 1 μm height, whereas for square and hexagonal lattices, the random patterns are limited to ~100 nm height.

IV. OPTICAL CHARACTERIZATION

We measured reflectance (R) of our samples to observe optical absorbance (A = 1 − R, T = 0 due to the thick GaAs substrate) for enhanced light trapping through photonic integration in GaAs. We present our results captured within the 450 nm–700 nm visible wavelength range in Figs. 8(a) and 8(b). We have used a 50× microscope objective with 0.7 NA to collect reflection and illuminate our samples over a wide angle of 45° that is integrated to a CCD array detector and spectrometer as presented in Ref. 37. We observed 31% reflectance or 79% absorbance from the bare GaAs substrate within 450 nm–700 nm, whereas the surface reflectance reduced drastically for photonic integrated GaAs nanowires. As evidenced from Fig. 8, a square lattice with 240 nm diameter presents 6.6% of reflectance (R) and 93.7% optical absorbance (1 − R);
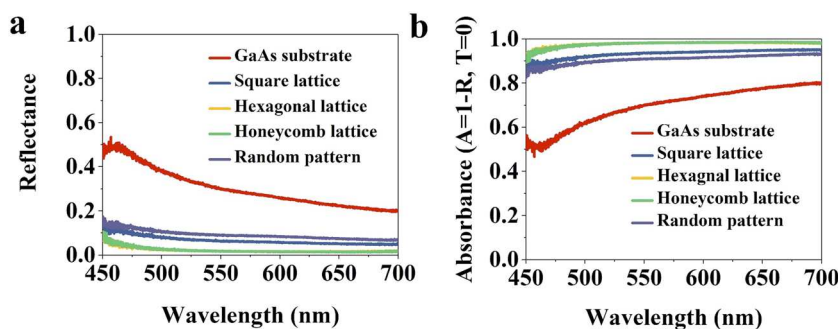
FIG. 8. Optical characterization of the fabricated photonic samples with a square lattice of 240 nm diameter, a hexagonal lattice of 240 nm diameter, a honeycomb lattice of 180 nm diameter, and random patterns obtained out of a hexagonal lattice of 180 nm diameter. (a) Reflectance (R) and (b) absorbance (A), where T is assumed to be zero due to the thick GaAs substrate.

a hexagonal lattice with 240 nm diameter shows 2.2% reflectance and 97.8% optical absorbance; and a honeycomb lattice with 180 nm diameter shows 2% reflectance or 98% optical absorbance from 450 nm to 700 nm. In the case of random lattice [Figs. 7(b) and 7(c)], we observe 9% reflectance or 91% absorbance. Therefore, we propose that hexagonal and honeycomb lattices are a better photonic integration scheme compared to square lattice and random patterns toward broadband and wide angle antireflection or absorption applicable in solar energy harvesting.

V. METHODS

A. Uniform photonic nanostructuring of variable lattices through electron beam lithography

We carried out photonic nanostructuring in GaAs through the hard mask and negative resist using variable dose-based electron beam lithography followed by plasma etching tools such as RIE and ICP. Square lattice, hexagonal lattice, and honeycomb lattice arrays with a range of design parameters and dose variations were designed using proprietary Raith GmbH pattern editing software. The design contains periodic square arrays of varying diameter from 180 nm to 360 nm within an overall periodicity of 300 nm or 400 nm. A clean GaAs substrate is coated with 300 nm–400 nm of SiO_2 for 5 min using plasma enhanced chemical vapor deposition (PECVD). The SiO_2/GaAs substrate was spin-coated with a 200 nm thick film of the negative electron beam resist AR-N-7520 and post-baked at $100\,^\circ C$ for 1 min to remove the liquid residues. The pattern was exposed with a Raith Voyager electron beam writer at an acceleration voltage of 50 kV and a beam current of ~213 pA for an exposure dose of 40 $\mu C/cm^2$. The exposed samples were then developed in AR 300-46 solvent for 1 min, followed by rinsing in iso-propyl alcohol (IPA). The developed pattern in the negative resist shows pillars of variable diameters and features depending upon doses and design parameters and type of lattice.

The reverse PR patterned SiO_2/GaAs substrate was etched using reactive ion etching for 19 min with CHF_3—40 SCCM at a pressure of 26 mTorr, RF power—80 W. The residual resist is then removed from the substrate using the Microposit 1165 resist remover followed by cleaning with acetone and IPA. Finally, the sample is cleaned with oxygen plasma for 5 min. We obtain variable features of the patterned SiO_2/GaAs depending upon the etch rate and design parameters. We perform 3 min–5 min ICP etching of the SiO_2 patterned to etch the underlying GaAs through the hard mask followed by HF etching of the hard mask to observe the underlying GaAs nanopatterning. The etching parameters were as follows: chlorine (Cl_2)—20 SCCM, argon (Ar)—10 SCCM, RF power—200 W, ICP power—300 W, and pressure—2.5 mTorr. The surface morphology of the realized photonic integrated patterns on SiO_2 and GaAs is studied using Raith field emission scanning electron microscopy (FESEM).

VI. CONCLUSION

We have presented a study including design and experiment on several photonic nanostructuring possibilities for photonic crystal integration over GaAs substrates such as square lattice, hexagonal lattice, and honeycomb lattice patterns through hard mask deposition, EBL patterning, RIE, and ICP etching. We could obtain periodic and uniform GaAs nanowires of diameter ~200 nm to 300 nm and a height of ~300 nm to 560 nm through our experiment. To present applications of the fabricated nanowires, we have carried out an FDTD-based simulation study on the optical properties such as electric field distribution, optical absorbance, and total optical absorbed power for square, hexagonal, and honeycomb lattice arrangements considering different design parameters. It is experimentally observed that hexagonal and honeycomb types of lattices show better absorbance properties, up to 98% over a broad (450 nm–700 nm) wavelength range. This study is aimed at obtaining uniform periodic GaAs nanowire photonic crystals or a template for uniform periodic growth of single GaAs nanowires per site with the help of surface patterning. The future application of such photonic crystals is that they can be used as a broadband absorber for efficiency improvement in solar cells.

DATA AVAILABILITY

The data that support the findings of this study are available within the article and from the corresponding author upon reasonable request.

REFERENCES

[1] R. Yan, D. Gargas, and P. Yang, "Nanowire photonics," Nat. Photonics **3**, 569 (2009).

[2] Q. G. Du, C. H. Kam, H. V. Demir, H. Y. Yu, and X. W. Sun, "Broadband absorption enhancement in randomly positioned silicon nanowire arrays for solar cell applications," Opt. Lett. **36**, 1884–1886 (2011).

[3] S. W. Eaton, A. Fu, A. B. Wong, C. Z. Ning, and P. Yang, "Semiconductor nanowire lasers," Nat. Rev. Mater. **1**, 16028 (2016).

[4] N. Huang, C. Lin, and M. L. Povinelli, "Broadband absorption of semiconductor nanowire arrays for photovoltaic applications," J. Opt. **14**, 024004 (2012).

[5] M. R. Philip, D. D. Choudhary, M. Djavid, K. Q. Le, J. Piao, and H. P. T. Nguyen, "High efficiency green/yellow and red InGaN/AlGaN nanowire light-emitting diodes grown by molecular beam epitaxy," J. Sci.: Adv. Mater. Devices **2**, 150–155 (2017).

[6] T. Kuykendall, P. J. Pauzauskie, Y. Zhang, J. Goldberger, D. Sirbuly, J. Denlinger, and P. Yang, "Crystallographic alignment of high-density gallium nitride nanowire arrays," Nat. Mater. **3**, 524 (2004).

[7] C. J. Barrelet, A. B. Greytak, and C. M. Lieber, "Nanowire photonic circuit elements," Nano Lett. **4**, 1981–1985 (2004).

[8] J. D. Joannopoulos, P. R. Villeneuve, and S. Fan, "Photonic crystals: Putting a new twist on the light," Nature **386**, 143 (1997).

[9] J. A. Czaban, D. A. Thompson, and R. R. LaPierre, "GaAs core-shell nanowires for photovoltaic applications," Nano Lett. **9**, 148–154 (2008).

[10] A. I. Hochbaum and P. Yang, "Semiconductor nanowires for energy conversion," Chem. Rev. **110**, 527–546 (2009).

[11] Z. V. Vardeny, A. Nahata, and A. Agrawal, "Optics of photonic quasicrystals," Nat. Photonics **7**, 177 (2013).

[12] J. Xavier, J. Probst, F. Back, P. Wyss, D. Eisenhauer, B. Löchel, E. Rudigier-Voigt, and C. Becker, "Quasicrystalline-structured light harvesting nanophotonic silicon films on nanoimprinted glass for ultra-thin photovoltaics," Opt. Mater. Express **4**, 2290–2299 (2014).

[13] M. A. Green, Y. Hishikawa, W. Warta, E. D. Dunlop, D. H. Levi, J. Hohl-Ebinger, and A. W. Ho-Baillie, "Solar cell efficiency tables (version 50)," Prog. Photovoltaics: Res. Appl. **25**, 668–676 (2017).

[14] C. P. Svensson, T. Mårtensson, J. Trägårdh, C. Larsson, M. Rask, D. Hessman, L. Samuelson, and J. Ohlsson, "Monolithic GaAs/InGaP nanowire light emitting diodes on silicon," Nanotechnology **19**, 305201 (2008).

[15] K. Tomioka, J. Motohisa, S. Hara, K. Hiruma, and T. Fukui, "GaAs/AlGaAs core multishell nanowire-based light-emitting diodes on Si," Nano Lett. **10**, 1639–1644 (2010).

[16] P. Krogstrup, H. I. Jørgensen, M. Heiss, O. Demichel, J. V. Holm, M. Aagesen, J. Nygard, and A. Fontcuberta i Morral, "Single-nanowire solar cells beyond the Shockley–Queisser limit," Nat. Photonics **7**, 306 (2013).

[17] G. Mariani, A. Scofield, and C. Hung, "GaAs nanopillar-array solar cells employing *in situ* surface passivation," Nat. Commun. **4**, 1497 (2013).

[18] M. Yao, N. Huang, S. Cong, C. Y. Chi, M. A. Seyedi, Y. T. Lin, Y. Cao, M. L. Povinelli, P. D. Dapkus, and C. Zhou, "GaAs nanowire array solar cells with axial p–i–n junctions," Nano Lett. **14**(6), 3293–3303 (2014).

[19] X. Dai, S. Zhang, Z. Wang, G. Adamo, H. Liu, Y. Huang, C. Couteau, and C. Soci, "GaAs/AlGaAs nanowire photodetector," Nano Lett. **14**, 2688–2693 (2014).

[20] G. E. Cirlin, V. G. Dubrovskii, Y. B. Samsonenko, A. D. Bouravleuv, K. Durose, Y. Y. Proskuryakov, B. Mendes, L. Bowen, M. A. Kaliteevski, R. A. Abram, and D. Zeze, "Self-catalyzed, pure zincblende GaAs nanowires grown on Si (111) by molecular beam epitaxy," Phys. Rev. B **82**, 035302 (2010).

[21] J. H. Paek, T. Nishiwaki, M. Yamaguchi, and N. Sawaki, "Catalyst free MBE-VLS growth of GaAs nanowires on (111) Si substrate," Phys. Status Solidi C **6**, 1436–1440 (2009).

[22] Y. Zhang, H. A. Fonseka, M. Aagesen, J. A. Gott, A. M. Sanchez, J. Wu, D. Kim, P. Jurczak, S. Huo, and H. Liu, "Growth of pure zinc-blende GaAs (P) core–shell nanowires with highly regular morphology," Nano Lett. **17**, 4946–4950 (2017).

[23] K. Ikejiri, J. Noborisaka, S. Hara, J. Motohisa, and T. Fukui, "Mechanism of catalyst-free growth of GaAs nanowires by selective area MOVPE," J. Cryst. Growth **298**, 616–619 (2007).

[24] T. Mårtensson, C. P. Svensson, B. A. Wacaser, M. W. Larsson, W. Seifert, K. Deppert, A. Gustafsson, L. R. Wallenberg, and L. Samuelson, "Epitaxial III–V nanowires on silicon," Nano Lett. **4**, 1987–1990 (2004).

[25] A. M. Munshi, D. L. Dheeraj, V. T. Fauske, D. C. Kim, J. Huh, J. F. Reinertsen, L. Ahtapodov, K. D. Lee, B. Heidari, A. T. Van Helvoort, and B. O. Fimland, "Position-controlled uniform GaAs nanowires on silicon using nanoimprint lithography," Nano Lett. **14**, 960–966 (2014).

[26] C. Lu and R. H. Lipson, "Interference lithography: A powerful tool for fabricating periodic structures," Laser Photonics Rev. **4**, 568–580 (2010).

[27] C. K. Ullal, M. Maldovan, E. L. Thomas, G. Chen, Y.-J. Han, and S. Yang, "Photonic crystals through holographic lithography: Simple cubic, diamond-like, and gyroid-like structures," Appl. Phys. Lett. **84**, 5434–5436 (2004).

[28] M. Deubel, G. von Freymann, M. Wegener, S. Pereira, K. Busch, and C. M. Soukoulis, "Direct laser writing of three-dimensional photonic-crystal templates for telecommunications," Nat. Mater. **3**, 444 (2004).

[29] J. Xu, Z. Wang, Z. Zhang, D. Wang, and Z. Weng, "Fabrication of moth-eye structures on silicon by direct six-beam laser interference lithography," J. Appl. Phys. **115**(20), 203101 (2014).

[30] S. Behera and J. Joseph, "Single-step optical realization of bio-inspired dual-periodic motheye and gradient-index-array photonic structures," Opt. Lett. **41**(15), 3579–3582 (2016).

[31] J. Xavier and J. Joseph, "Tunable complex photonic chiral lattices by reconfigurable optical phase engineering," Opt. Lett. **36**, 403–405 (2011).

[32] S. Behera, M. Kumar, and J. Joseph, "Submicrometer photonic structure fabrication by phase spatial-light-modulator-based interference lithography," Opt. Lett. **41**, 1893–1896 (2016).

[33] S. Behera and J. Joseph, "Design and fabrication of woodpile photonic structures through phase SLM-based interference lithography for omnidirectional optical filters," Opt. Lett. **42**, 2607–2610 (2017).

[34] S. Behera and J. Joseph, "Design and realization of functional metamaterial basis structures through optical phase manipulation-based interference lithography," J. Opt. **19**, 105103 (2017).

[35] Y. Kanamori, M. Sasaki, and K. Hane, "Broadband antireflection gratings fabricated upon silicon substrates," Opt. Lett. **24**, 1422–1424 (1999).

[36] N. Liu, H. Guo, L. Fu, S. Kaiser, H. Schweizer, and H. Giessen, "Three-dimensional photonic metamaterials at optical frequencies," Nat. Mater. **7**, 31 (2008).

[37] S. Behera, P. W. Fry, H. Francis, C. Y. Jin, and M. Hopkinson, "Broadband, wide-angle antireflection in GaAs through surface nano-structuring for solar cell applications," Sci. Rep. **10**, 1–10 (2020).